GKSS
FORSCHUNGSZENTRUM
in der HELMHOLTZ-GEMEINSCHAFT

Preprint 2010

Variationally consistent modeling of finite strain plasticity theory with non-linear kinematic hardening

J. Mosler

This is a preprint of an article accepted by:

Computer Methods in Applied Mechanics and Engineering

(2010)

GKSS Research Centre Geesthacht
Materials Mechanics

Variationally consistent modeling of finite strain plasticity theory with non-linear kinematic hardening

J. Mosler

Materials Mechanics
Institute for Materials Research
GKSS Research Centre
D-21502 Geesthacht, Germany
E-Mail: joern.mosler@gkss.de

SUMMARY

Variational constitutive updates provide a physically and mathematically sound framework for the numerical implementation of material models. In contrast to conventional schemes such as the return-mapping algorithm, they are directly and naturally based on the underlying variational principle. Hence, the resulting numerical scheme inherits all properties of that principle. In the present paper, focus is on a certain class of those variational methods which relies on energy minimization. Consequently, the algorithmic formulation is governed by energy minimization as well. Accordingly, standard optimization algorithms can be applied to solve the numerical problem. A further advantage compared to conventional approaches is the existence of a natural distance (semi metric) induced by the minimization principle. Such a distance is the foundation for error estimation and as a result, for adaptive finite elements methods. Though variational constitutive updates are relatively well developed for so-called *standard dissipative solids*, i.e., solids characterized by the normality rule, the more general case, i.e., *generalized standard materials*, is far from being understood. More precisely, (Int. J. Sol. Struct. 2009, **46**:1676–1684) represents the first step towards this goal. In the present paper, a variational constitutive update suitable for a class of nonlinear kinematic hardening models at finite strains is presented. Two different prototypes of Armstrong-Frederick type are re-formulated into the aforementioned variationally consistent framework. Numerical tests demonstrate the consistency of the resulting implementation.

1 Introduction

One of the cornerstones of mechanics, or more precisely, of physics in general, are without doubt variational principles. Even more explicitly: "Some authors believe that variational principles are the foundation of physics", see [1]. The probably best known example is given by the principle of least action a.k.a. the principle of extremal action as originally advocated by Maupertuis. That principle was further elaborated and extended and led finally to the most frequently applied methods in continuum mechanics. Among them are the principle of virtual work and Hamilton's principle. For conservative systems such as elastic bodies, stationarity principles can usually be recast into equivalent minimization problems. For instance, the principle of virtual work defines then a state of minimum potential. However, also for dissipative processes, minimization principles can be developed.

This is not self-evident, since the equations of motion are not self-adjoint in this case, cf. [2]. One such principle in thermodynamics is the postulate of maximum dissipation, cf. [3, 4]. It will play an important role in the present paper [2].

Besides their mathematical and physical elegance, variational principles, show several additional advantages compared to other approaches. From a physical point of view, the applicability of Noether's theorem is for instance important, cf. [5]. In case of minimization principles, the advantages are even more pronounced. In this connection, it is referred to the framework of Γ-convergence [6, 7]. Frequently, this framework represents the only avenue for analyzing the existence of solutions, cf. [8]. In addition to the aforementioned advantages, minimization problems are very interesting from a computational point of view as well. For example, such principles can be taken as a canonical basis for error estimation, cf. [9–12] and furthermore, they open up the possibility of applying state of the art optimization algorithms. Particularly for non-smooth problems such as those in plasticity theory, this represents an interesting feature, [13].

Though variational principles, or more specifically minimization problems, are very promising, their derivation is oftentimes difficult. Equally importantly, even if such a principle has been found, its transfer to a computational method is in many cases not straightforward. Certainly, the finite element method based on the principle of virtual work, or Ritz method relying on the postulate of minimum potential energy are the best known counterexamples. But regarding Hamilton's principle or the postulate of maximum dissipation, the opposite is true. Only relatively recently, time integration schemes in line with the underlying variational principles were proposed, cf. [14, 15]. The same holds for the implementation of constitutive models governed by associative evolution equations, i.e., *standard dissipative solids* in the sense of Halphen & Nguyen [16], cf. [11, 13, 17–19]. In contrast to conventional (non-variational) algorithmic formulations, variationally consistent numerical models are governed by their underlying variational principle and thus, they inherit all of their properties like energy conservation. This is why they are physically sound and very powerful.

The present paper is concerned with so-called *variational constitutive updates*, cf. [11, 13, 17–21]. These updates make use of the postulate of maximum dissipation and allow to compute all state variables, together with the unknown deformation mapping, by minimizing a suitable energy functional. Also, such methods allow to analyze the existence of solutions by using nowadays standard tools such as those known from hyperelasticty [20, 22, 23], and they can be applied as a canonical basis for error estimation, cf. [9–12].

Concerning associative evolution equations (standard dissipative solids), variational updates are relatively well understood. For rate-independent models, a general numerical framework suitable for their implementation was advocated in [24]. It can be applied to almost all (possibly anisotropic) plasticity models including arbitrary isotropic and linear kinematic hardening. In case of rate-dependent viscous-type constitutive laws, a numerical implementation can be found in [25].

Clearly for many applications, non-associative evolution equations are required. This is typical for models in soil-mechanics. Even though most of such models can be described within the framework of *generalized standard materials* [26, 27], no governing variational principle exists. Therefore, no general variational constitutive update for those models has been proposed yet. In [28], a first step towards this extension is discussed. More precisely, a Drucker-Prager-type model based on a volumetric/deviatoric split of the Helmholtz energy, the yield function and the plastic potential was considered. Without going too much into detail, the resulting variational structure is closely related to the orthogonality between the spaces of deviatoric and hydrostatic tensors. Consequently, this approach is

very specific and thus, it cannot serve as prototype for other kinds of material laws.

In the present paper, focus is on a variational description of non-linear kinematic hardening at finite strains. Such hardening type is necessary for capturing the Bauschinger effect which is mandatory for describing the hysteresis in load reversals particularly for metals, cf. [29]. Similarly to the aforementioned Drucker-Prager-type model, non-linear kinematic hardening does not obey the (classical) postulate of maximum dissipation. Hence, there is no associated variational principle. Therefore, new modeling techniques have to be developed.
Although non-linear kinematic, or more precisely, Armstrong-Frederick-type hardening [30], is well established for linearized kinematics, the variety of its geometrically non-linear extensions is numerous, cf. [31]. For this reason, two different versions of non-linear kinematic hardening are considered in this paper and recast into an equivalent variational framework. The first of those is based on a standard evolution equation of the back stress within the intermediate configuration induced by a multiplicative decomposition of the deformation gradient, see model A in [31]. The latter makes use of the so-called *center configuration*, originally proposed in [32] (see also [33] for further elaborations). Similar ideas have been advocated earlier in [34].
Conceptually, the novel variational constitutive updates presented here are based on a more general form of the postulate of maximum dissipation. However and in contrast to associative plasticity theory, the non-associative evolution equations are enforced explicitly. This constrained extremal principle is finally recast into an equivalent unconstrained counterpart by utilizing a suitable parameterization of the flow rule and the evolution equation governing the back stress, cf. [28].

The paper is organized as follows: Section 2 is concerned with a brief introduction to finite strain plasticity based on associated evolution equations. Particularly, the governing variational structure is emphasized and the implementation by means of variational constitutive updates is presented. In Section 3, two different types of non-linear kinematic hardening are discussed. While the first of those is defined by a standard evolution equation with respect to the intermediate configuration, the second model is related to the concept of a center configuration. A variationally consistent re-formulation of such models, together with their numerical implementation, is elaborated in Section 4. The applicability of the resulting algorithmic formulations are highlighted in Section 5.

2 Variational updates for associative finite strain plasticity theory

This section is concerned with a concise review of variational constitutive updates suitable for the modeling of *standard dissipative solids* in the sense of Halphen & Nguyen [16]. Assuming normality rules, i.e., associative evolution equations, such updates allow to compute all state variables, together with the unknown deformation, jointly by minimizing the stress power of the respective mechanical system, cf. [11, 13, 20, 21]. While the variational structure of finite strain plasticity is briefly discussed in Subsection 2.1, a short note on the respective implementation is given in Subsection 2.2.

2.1 Fundamentals

In line with Lee [35], a multiplicative decomposition of the deformation gradient $\boldsymbol{F} := \mathrm{GRAD}\boldsymbol{\varphi}$ into an elastic part $\boldsymbol{F}^{\mathrm{e}}$ and a plastic part $\boldsymbol{F}^{\mathrm{p}}$ of the type

$$\boldsymbol{F} = \boldsymbol{F}^{\mathrm{e}} \cdot \boldsymbol{F}^{\mathrm{p}}, \qquad \text{with} \qquad \det \boldsymbol{F}^{\mathrm{e}} > 0,\ \det \boldsymbol{F}^{\mathrm{p}} > 0 \tag{1}$$

is postulated. Based on this split, an additive decomposition of the Helmholtz energy

$$\Psi = \Psi^{\mathrm{e}}(\boldsymbol{F}^{\mathrm{e}}) + \Psi^{\mathrm{p}}(\boldsymbol{\alpha}) \tag{2}$$

is adopted, cf. [36–38]. In Eq. (2), $\boldsymbol{\alpha} \in \mathbb{R}^n$ is a strain-like internal variable (or a suitable set) related to plastic hardening and Ψ^{p} denotes the associated stored energy. Clearly, Eq. (2) implies that plastic effects do not affect the elastic response, i.e., no material degradation is present. Inserting assumptions (1) and (2) into the dissipation inequality yields for isothermal processes

$$\mathcal{D} = \left(\boldsymbol{F}^{\mathrm{p}} \cdot \boldsymbol{S} \cdot \boldsymbol{F}^{p^T} - 2\, \frac{\partial \Psi}{\partial \boldsymbol{C}^{\mathrm{e}}} \right) : \frac{1}{2}\, \dot{\boldsymbol{C}}^{\mathrm{e}} + \boldsymbol{S} : \left(\boldsymbol{F}^{\mathrm{p}^T} \cdot \boldsymbol{C}^{\mathrm{e}} \cdot \dot{\boldsymbol{F}}^{\mathrm{p}} \right) + \boldsymbol{Q} \cdot \dot{\boldsymbol{\alpha}} \geq 0. \tag{3}$$

Here and henceforth, $\boldsymbol{C}^{\mathrm{e}} := \boldsymbol{F}^{\mathrm{e}T} \cdot \boldsymbol{F}^{\mathrm{e}}$, $\boldsymbol{P}$, $\boldsymbol{S} := \boldsymbol{F}^{-1} \cdot \boldsymbol{P}$ and $\boldsymbol{Q} := -\partial_{\boldsymbol{\alpha}} \Psi$ represent the elastic right Cauchy-Green strain tensor, the first Piola-Kirchhoff stress tensor, the second Piola-Kirchhoff stress tensor and a stress-like internal variable work conjugate to $\boldsymbol{\alpha}$, respectively. Application of the by now standard Colemann & Noll procedure [39–41], gives the stress response

$$\boldsymbol{S} = 2\, \frac{\partial \Psi}{\partial \boldsymbol{C}} = 2\, \boldsymbol{F}^{\mathrm{p}^{-1}} \cdot \frac{\partial \Psi}{\partial \boldsymbol{C}^{\mathrm{e}}} \cdot \boldsymbol{F}^{\mathrm{p}^{-T}} \tag{4}$$

and the reduced dissipation inequality

$$\mathcal{D} = \boldsymbol{\Sigma} : \boldsymbol{L}^{\mathrm{p}} + \boldsymbol{Q} \cdot \dot{\boldsymbol{\alpha}} \geq 0 \tag{5}$$

with $\boldsymbol{\Sigma} = 2\, \boldsymbol{C}^{\mathrm{e}} \cdot \partial_{\boldsymbol{C}^{\mathrm{e}}} \Psi$ being the Mandel stresses (cf. [26]) and $\boldsymbol{L}^{\mathrm{p}} = \dot{\boldsymbol{F}}^{\mathrm{p}} \cdot \boldsymbol{F}^{\mathrm{p}^{-1}}$ denoting the plastic velocity gradient. Both objects belong to the intermediate configuration.

For defining admissible stresses, the elastic domain denoted as $\mathbb{E}_{\boldsymbol{\sigma}}$ is introduced. In line with the dissipation inequality (5), $\mathbb{E}_{\boldsymbol{\sigma}}$ is formulated in terms of $\boldsymbol{\Sigma}$. More precisely,

$$\mathbb{E}_{\boldsymbol{\sigma}} = \left\{ (\boldsymbol{\Sigma}, \boldsymbol{Q}) \in \mathbb{R}^{9+n} \;\middle|\; \phi(\boldsymbol{\Sigma}, \boldsymbol{Q}) \leq 0 \right\}. \tag{6}$$

Clearly, the yield function ϕ spanning that space has to comply with experimental data and has to fulfill certain regularity conditions, cf. [42]. Since in this paper focus is on nonlinear kinematic hardening models, a family of yield functions of the type

$$\phi(\boldsymbol{\Sigma}, \boldsymbol{Q}^{\mathrm{k}}) = \Sigma^{\mathrm{eq}}(\boldsymbol{\Sigma} - \boldsymbol{Q}^{\mathrm{k}}) - Q_{\mathrm{i}} - Q_0^{\mathrm{eq}} \tag{7}$$

is considered. In Eq. (7), $\boldsymbol{Q}^{\mathrm{k}} = \boldsymbol{Q}^{\mathrm{k}}(\boldsymbol{\alpha}^{\mathrm{k}})$, $Q_{\mathrm{i}} = Q_{\mathrm{i}}(\alpha_{\mathrm{i}})$, Σ^{eq} and Q_0^{eq} are the back stress tensor related to kinematic hardening, a scalar-valued, stress-like internal variable governing the isotropic counterpart, an equivalent stress measure defining the shape of the yield function ϕ and the radius of the initial elastic domain $\mathbb{E}_{\boldsymbol{\sigma}}$, respectively.

Canonical or associative evolution equations can be derived in a physically and mathematically elegant manner by enforcing the postulate of maximum dissipation

$$\sup_{(\boldsymbol{\Sigma}, \boldsymbol{Q}^{\mathrm{k}}, Q_{\mathrm{i}}) \in E_{\boldsymbol{\sigma}}} \mathcal{D} \tag{8}$$

leading finally to

$$\boldsymbol{L}^{\mathrm{p}} = \lambda\, \partial_{\boldsymbol{\Sigma}}\phi \qquad \dot{\boldsymbol{\alpha}}^{\mathrm{k}} = \lambda\, \partial_{\boldsymbol{Q}^{\mathrm{k}}}\phi \qquad \alpha_{\mathrm{i}} = \lambda, \tag{9}$$

together with the classical Karush-Kuhn-Tucker conditions $\lambda \geq 0$, $\lambda\, \phi \geq 0$. According to Eq. $(9)_2$, the postulate of maximum dissipation implies linear kinematic hardening. Hence, this principle has to be modified, if nonlinear hardening of Armstrong-Frederick type is to be modeled. Such an enhanced principle is elaborated in the next sections. Furthermore, it should be noted in advance that other, modified evolution equations for the internal variable $\boldsymbol{\alpha}$ based on objective time derivatives can be applied as well. This will be briefly discussed in the next section.

In what follows, the finite strain plasticity model discussed before is re-written into a variational form, cf. [13, 20, 24]. It bears emphasis that the finally presented parameterization is new. Though it is in line with the one introduced in [24, 28], it is applied directly to the analytical, i.e., to the continuous, problem. In [24, 28], it has only been elaborated for the algorithmic formulation. In this respect, the current derivation is more consistent, since it is based on a unique framework. Conceptually, the variational form of plasticity is based on the stationarity of the stress power

$$\begin{aligned} \tilde{\mathcal{E}}(\dot{\boldsymbol{\varphi}}, \dot{\boldsymbol{F}}^{\mathrm{p}}, \dot{\boldsymbol{\alpha}}, \boldsymbol{\Sigma}, \boldsymbol{Q}) &:= \boldsymbol{P} : \dot{\boldsymbol{F}} + J & (10)\\ &= \dot{\Psi}(\dot{\boldsymbol{\varphi}}, \dot{\boldsymbol{F}}^{\mathrm{p}}, \dot{\boldsymbol{\alpha}}) + \mathcal{D}(\dot{\boldsymbol{F}}^{\mathrm{p}}, \dot{\boldsymbol{\alpha}}, \boldsymbol{\Sigma}, \boldsymbol{Q}) + J, & (11) \end{aligned}$$

cf.[13, 20]. Here, $J = J(\boldsymbol{\Sigma}, \boldsymbol{Q})$ is the characteristic function of $\mathbb{E}_{\boldsymbol{\sigma}}$ with $\boldsymbol{Q} := \{\boldsymbol{Q}^{\mathrm{k}}, Q_{\mathrm{i}}\}$ and $\boldsymbol{\alpha} := \{\boldsymbol{\alpha}^{\mathrm{k}}, \alpha_{\mathrm{i}}\}$. Hence, for admissible stresses J vanishes, while inadmissible states are penalized by $J = \infty$. Applying the postulate of maximum dissipation (maximization of $\tilde{\mathcal{E}}$ with respect to the stress-like variables) yields

$$\mathcal{E}(\dot{\boldsymbol{\varphi}}, \dot{\boldsymbol{F}}^{\mathrm{p}}, \dot{\boldsymbol{\alpha}}) = \dot{\Psi}(\dot{\boldsymbol{\varphi}}, \dot{\boldsymbol{F}}^{\mathrm{p}}, \dot{\boldsymbol{\alpha}}) + J^*(\dot{\boldsymbol{L}}^{\mathrm{p}}, \dot{\boldsymbol{\alpha}}) \tag{12}$$

with J^* being the Legendre transformation of J. For admissible stress states and associative evolution equations, J^* is the dissipation. Generally, the computation of this transformation is not trivial. However, for a broad class of plasticity models frequently applied in solids mechanics, the equivalent stress in Eq. (7) is a positively homogeneous function of degree one. In that case, a closed-form solution can be derived in a straightforward manner, i.e., $J^* = \lambda\, Q_0^{\mathrm{eq}}\ \forall (\boldsymbol{\Sigma}, \boldsymbol{Q}) \in \mathbb{E}_\sigma$, cf. [13, 20, 24].

Recently, a novel implementation for variational constitutive updates was advocated in [24, 28]. The underlying key idea is to parameterize the restrictions imposed by the flow rule conveniently. More precisely, using associative evolution equations, i.e,

$$\dot{\boldsymbol{F}}^{\mathrm{p}} \cdot \boldsymbol{F}^{\mathrm{p}\,-1} = \lambda\, \partial_{\boldsymbol{\Sigma}}\phi \tag{13}$$

the rate of plastic strains can be decomposed into a direction $\partial_{\boldsymbol{\Sigma}}\phi$ and an amplitude λ. Consequently, a suitable description of the flow rule relies crucially on a convenient parameterization of the flow direction $\partial_{\boldsymbol{\Sigma}}\phi$. For instance, a von Mises-type model is defined by the following constraints.

$$\partial_{\boldsymbol{\Sigma}}\phi = \frac{\mathrm{dev}\boldsymbol{\Sigma}}{||\mathrm{dev}\boldsymbol{\Sigma}||} \in \mathcal{M} := \left\{ \boldsymbol{M} \;\middle|\; \boldsymbol{M} = \boldsymbol{M}^T,\ \mathrm{tr}\boldsymbol{M} = 0,\ \boldsymbol{M} : \boldsymbol{M} = 1 \right\}. \tag{14}$$

In [13], such constraints have been incorporated by adopting Lagrange multipliers. Here and in line with [24, 28], a different approach is emphasized. Conceptually, pseudo stresses $\tilde{\boldsymbol{\Sigma}}$ are introduced. They are not necessarily identical to their (relative) physical counterparts, i.e., $\tilde{\boldsymbol{\Sigma}} \neq \boldsymbol{\Xi} := \boldsymbol{\Sigma} - \boldsymbol{Q}^{\mathrm{k}}$, but they result (by definition) in the same physical flow

direction, i.e., $\partial_{\boldsymbol{\Sigma}}\phi|_{\boldsymbol{\Xi}} = \partial_{\boldsymbol{\Sigma}}\phi|_{\tilde{\boldsymbol{\Sigma}}}$. Using such pseudo stresses and focusing again for the sake of concreteness on von Mises type-models, the set $\mathcal{M}$ defining the physical constraints imposed by the flow rule can be re-written as

$$\mathcal{M} = \left\{ \frac{\text{dev}\tilde{\boldsymbol{\Sigma}}}{||\text{dev}\tilde{\boldsymbol{\Sigma}}||} \;\middle|\; \tilde{\boldsymbol{\Sigma}} = \tilde{\boldsymbol{\Sigma}}^T \right\} \tag{15}$$

and thus, the determination of the flow direction results in finding the proper symmetric second-order tensor $\tilde{\boldsymbol{\Sigma}}$. As a result, the constraints (14) can be a priori enforced (more precisely, they are naturally included). Employing such a parameterization, the functional dependency of the stress power is given by $\mathcal{E} = \mathcal{E}(\dot{\boldsymbol{\varphi}}, \tilde{\boldsymbol{\Sigma}}, \lambda)$. Then, according to [24, 28], it can be shown that all unknown state variables, together with the deformation mapping, follow jointly from minimizing the potential $\mathcal{E}$, i.e.,

$$(\dot{\boldsymbol{\varphi}}, \tilde{\boldsymbol{\Sigma}}, \lambda) = \arg \inf_{\tilde{\boldsymbol{\Sigma}},\lambda} \mathcal{E}(\dot{\boldsymbol{\varphi}}, \tilde{\boldsymbol{\Sigma}}, \lambda). \tag{16}$$

Since such schemes are, despite their efficiency and mathematical and physical elegance, nowadays still not standard, the validity of the minimization principle (16) is briefly shown in what follows. For that purpose, it is proved that the stationarity condition of $\mathcal{E}$ with respect to $\tilde{\boldsymbol{\Sigma}}$ and λ complies completely with the underlying associative plasticity model. Since for that purpose, the partial derivatives of $\mathcal{E}$ with respect to $\tilde{\boldsymbol{\Sigma}}$ and λ are considered, the deformation mapping is assumed as constant without loss of generality, i.e.,

$$\boldsymbol{\varphi} = \text{const} \quad \Rightarrow \quad \dot{\boldsymbol{F}} = \boldsymbol{0} \quad \Rightarrow \quad \dot{\boldsymbol{F}}^{\text{e}} = -\boldsymbol{F}^{\text{e}} \cdot \boldsymbol{L}^{\text{p}}. \tag{17}$$

As a result, the stress power reads

$$\mathcal{E} = \dot{\Psi} + \mathcal{D} = -\left(\boldsymbol{F}^{\text{e}T} \cdot \frac{\partial \Psi^{\text{e}}}{\partial \boldsymbol{F}^{\text{e}}} \right) : \boldsymbol{L}^{\text{p}} + \lambda\, \boldsymbol{Q}^{\text{k}} : \boldsymbol{L}^{\text{p}} + \lambda\, Q_{\text{i}} + \lambda\, Q_0^{\text{eq}} \tag{18}$$

for a combined isotropic/kinematic hardening model. Hence, the stationarity condition with respect to the plastic multiplier is obtained as

$$\begin{array}{rcl} \delta_\lambda \mathcal{E} & = & \left\{ -\boldsymbol{\Sigma} : \partial_{\boldsymbol{\Sigma}}\phi|_{\tilde{\boldsymbol{\Sigma}}} + \boldsymbol{Q}^{\text{k}} : \partial_{\boldsymbol{\Sigma}}\phi|_{\tilde{\boldsymbol{\Sigma}}} + Q_{\text{i}} + Q_0^{\text{eq}} \right\}\, \delta\lambda = 0 \\ & \Leftrightarrow & -\phi = 0. \end{array} \tag{19}$$

Accordingly, the resulting Euler-Lagrange equation enforces the yield function. Finally, a variation with respect to the pseudo stresses leads to

$$\begin{array}{rcl} \delta_{\tilde{\boldsymbol{\Sigma}}} \mathcal{E} & = & \lambda\, \left\{ -\boldsymbol{\Sigma} : \partial^2_{\boldsymbol{\Sigma}}\phi|_{\tilde{\boldsymbol{\Sigma}}} + \boldsymbol{Q}^{\text{k}} : \partial^2_{\boldsymbol{\Sigma}}\phi|_{\tilde{\boldsymbol{\Sigma}}} \right\} : \delta\tilde{\boldsymbol{\Sigma}} = 0 \\ & \Leftrightarrow & \boldsymbol{\Xi} : \partial^2_{\boldsymbol{\Xi}}\phi = 0. \end{array} \qquad \boldsymbol{\Xi} := \boldsymbol{\Sigma} - \boldsymbol{Q}^{\text{k}}. \tag{20}$$

In what follows, only positively homogeneous yield functions of degree one will be considered (more precisely, the equivalent stress Σ^{eq} is positively homogeneous of degree one). According to [28], for such yield functions, the flow rule obeys Eq. (20) exactly. As a consequence, the variational principle (16) indeed naturally includes the flow direction as well.

Once the minimization problem $\inf_{\tilde{\boldsymbol{\Sigma}},\lambda} \mathcal{E}$ has been solved, the stresses $\boldsymbol{P}$ can be computed from the reduced potential, i.e.,

$$\boldsymbol{P} = \partial_{\dot{\boldsymbol{F}}} \inf_{\tilde{\boldsymbol{\Sigma}},\lambda} \mathcal{E}. \tag{21}$$

Further details can be found in [24, 28].

2.2 Numerical implementation

Conceptually, variational constitutive updates are simply an approximation of the minimization problem (16). A first step towards this approximation is obtained by applying a time integration to the stress power $\mathcal{E}(\dot{\boldsymbol{\varphi}}, \tilde{\boldsymbol{\Sigma}}, \lambda)$, i.e.,

$$(\Delta\lambda, \tilde{\boldsymbol{\Sigma}}) = \arg \inf_{\Delta\lambda, \tilde{\boldsymbol{\Sigma}}} I_{\text{inc}}, \tag{22}$$

with

$$I_{\text{inc}} = \int_{t_n}^{t_{n+1}} \mathcal{E}(\dot{\boldsymbol{\varphi}}, \tilde{\boldsymbol{\Sigma}}, \lambda)\, \mathrm{d}t = \Psi_{n+1} - \Psi_n + Q_0^{\text{eq}}\, \Delta\lambda. \tag{23}$$

Here, the notations $\Delta\lambda := \int_{t_n}^{t_{n+1}} \lambda\, \mathrm{d}t$ and $(\bullet)_n := (\bullet)(t_n)$ have been introduced. Furthermore, a positively homogeneous yield function of degree one resulting in the dissipation $\mathcal{D} = \lambda\, Q_0^{\text{eq}}$ has been assumed. Since $\mathcal{E}$ is highly non-linear, the definition of the incrementally defined potential I_{inc} requires a proper time integration scheme. In this respect, the minimization problem (22) is not unique. However, if a consistent time integration is applied, consistency of the variational update is indeed guaranteed, i.e., the algorithm converges to the original problem (16), if $\Delta t \to 0$. One such consistent approximation is given by the first-order scheme

$$\begin{array}{lcl} \boldsymbol{F}_{n+1}^{\text{p}} & = & \exp\left[\Delta\lambda\ \partial_{\boldsymbol{\Sigma}}\phi|_{\tilde{\boldsymbol{\Sigma}}}\right] \cdot \boldsymbol{F}_n^{\text{p}} \\ \alpha_{\text{i}}|_{n+1} & = & \alpha_{\text{i}}|_n - \Delta\lambda \\ \boldsymbol{\alpha}_{\text{k}}|_{n+1} & = & \boldsymbol{\alpha}_{\text{k}}|_n - \Delta\lambda\ \partial_{\boldsymbol{\Sigma}}\phi|_{\tilde{\boldsymbol{\Sigma}}}\,. \end{array} \tag{24}$$

By inserting Eqs. (24) into the integrated stress power, the incremental potential

$$I_{\text{inc}}(\boldsymbol{F}_{n+1}, \tilde{\boldsymbol{\Sigma}}, \Delta\lambda) = \Psi_{n+1}(\boldsymbol{F}_{n+1}, \tilde{\boldsymbol{\Sigma}}, \Delta\lambda) - \Psi_n + Q_0^{\text{eq}}\, \Delta\lambda \tag{25}$$

is obtained. Most frequently and in line with classical computational plasticity theory [37, 38], the minimization problem $\inf I_{\text{inc}}$ is solved in a staggered fashion. More precisely, at a certain material point (the integration point), the material response is computed by keeping the deformation mapping fixed ($\boldsymbol{F} = \text{const}$, compare to the return-mapping algorithm, cf. [37, 38]). Hence, the problem

$$(\Delta\lambda, \tilde{\boldsymbol{\Sigma}}) = \arg \inf_{\Delta\lambda, \tilde{\boldsymbol{\Sigma}}} I_{\text{inc}}|_{\boldsymbol{F}=\text{const}} \tag{26}$$

is considered which gives rise to the introduction of the reduced potential

$$I_{\text{inc}}^{\text{red}}(\boldsymbol{F}) = \inf_{\Delta\lambda, \tilde{\boldsymbol{\Sigma}}} I_{\text{inc}}|_{\boldsymbol{F}=\text{const}}. \tag{27}$$

This potential, in turn, defines the stress response, i.e.,

$$\boldsymbol{P} = \partial_{\boldsymbol{F}} I_{\text{inc}}^{\text{red}}, \tag{28}$$

compare to Eq. (21). In contrast to the locally defined problem (26), the computation of the deformation mapping of the body Ω necessary for determining the stresses requires a globally conforming description, e.g., by adopting a finite element discretization. More precisely, the problem

$$\boldsymbol{\varphi} = \arg\inf \int_{\Omega} I_{\text{inc}}^{\text{red}}\, \mathrm{d}V \tag{29}$$

is to be solved. In case of externally applied forces, the energy from such work has to be considered as usual. It bears emphasis that problem (29) is equivalent to the principle of virtual work. Further details are omitted. They can be found in [13, 20, 24, 28].

3 Finite strain plasticity theory with non-linear kinematic hardening

This section is concerned with the fundamentals of non-linear kinematic hardening at finite strains. More precisely, two different models of Armstrong-Frederick-type [30] are presented. While a rather straightforward extension of the geometrically linearized case is addressed in Section 3.1, a model relying of the concept of a center configuration is discussed in Section 3.2, cf. [32].
According to Section 2, isotropic hardening obeys the postulate of maximum dissipation. Hence, it is not critical for further considerations and therefore, it can be neglected for the sake of simplicity here.

3.1 Model I

The first model suitable for the simulation of non-linear kinematic hardening of Armstrong-Frederick-type at finite strains can be considered as a straightforward extension of the original model [30]. While in Paragraph 3.1.1 the fundamentals are briefly discussed, a (standard) numerical implementation based on the return-mapping scheme is sketched in Paragraph 3.1.2.

3.1.1 Fundamentals

Analogously to the class of models analyzed in Section 2, a multiplicative decomposition of the deformation gradient and an additive split of the Helmholtz energy are assumed, i.e.,

$$\Psi = \Psi^{\mathrm{e}}(\boldsymbol{C}^{\mathrm{e}}) + \Psi^{\mathrm{p}}(\boldsymbol{\alpha}), \quad \Psi^{\mathrm{p}} = \frac{1}{2}\, c\, \boldsymbol{\alpha} : \boldsymbol{\alpha}. \tag{30}$$

Furthermore, according to Eq. (30), a quadratic function has been chosen for describing the effects due to non-linear hardening. Here and henceforth, $\boldsymbol{\alpha}$ is a strain-like variable energetically conjugate to the back stress $\boldsymbol{Q}$. Since isotropic hardening is neglected for the sake of simplicity, the indices k (kinematic) and i (isotropic) are not necessary anymore. Based on Eq. (30), the reduced dissipation inequality

$$\mathcal{D} = \boldsymbol{\Sigma} : \boldsymbol{L}^{\mathrm{p}} + \boldsymbol{Q} : \dot{\boldsymbol{\alpha}} \geq 0, \quad \boldsymbol{Q} := -\partial_{\boldsymbol{\alpha}} \Psi^{\mathrm{p}} = -c\, \boldsymbol{\alpha} \tag{31}$$

is derived. According to Eq. (31) the material time derivative of $\boldsymbol{\alpha}$ naturally appears. It is well known that evolution equations for the back strain depending on that time derivative might lead to unphysical results, cf. [43]. For this reason, modified equations based on objective time derivatives are frequently applied, see [31] and references cited therein. However, it bears emphasis that simply replacing $\dot{\boldsymbol{\alpha}}$ by an objective counterpart would change the physical dissipation and hence, such a procedure is not physical at all. However, if the condition of isotropy of $\Psi^{\mathrm{p}}(\boldsymbol{\alpha})$ is taken into account, the material time derivative can be related to an objective time derivative. More precisely,

$$\dot{\Psi}^{\mathrm{p}} = \boldsymbol{Q} : \dot{\boldsymbol{\alpha}} = \boldsymbol{Q} : \mathcal{P}_{\triangleright}(\dot{\overline{\mathcal{P}^{\triangleleft}(\boldsymbol{\alpha})}}), \tag{32}$$

cf. [44]. In Eq. (32), $\mathcal{P}_{\triangleright}(\boldsymbol{\alpha})$ and $\mathcal{P}^{\triangleleft}(\boldsymbol{\alpha})$ denote a push-forward and a pull-back operation of $\boldsymbol{\alpha}$ with respect to a certain configuration, cf. [5]. Depending on that configuration $\mathcal{P}_{\triangleright}(\dot{\overline{\mathcal{P}^{\triangleleft}(\boldsymbol{\alpha})}})$ can represent a convective time derivative such as a Lie-derivative or a co-rotational time derivative such as the Jaumann derivative, see [44, 45]. Eq. (32) is a direct

consequence, of the covariance of Ψ^{p}, cf. [5, 44]. For further details, the reader is referred to [44] and [45].

In line with the previous section, the space of admissible stresses is defined by means of a yield function

$$\phi = \Sigma^{\mathrm{eq}}(\boldsymbol{\Sigma} - \boldsymbol{Q}) - Q_0^{\mathrm{eq}} \tag{33}$$

which in turn depends on an equivalent stress measure Σ^{eq} being a positively homogeneous function of degree one. In the numerical examples presented in Section 5, a von Mises yield function of the type

$$\phi = ||\mathrm{dev}(\boldsymbol{\Sigma}) - \boldsymbol{Q}|| - Q_0^{\mathrm{eq}} \tag{34}$$

is adopted. In contrast to Section 2, different evolution equations than those induced by ϕ are considered here. Following the framework of generalized standard materials [26, 27] a plastic potential $\Omega \neq \phi$ is introduced and the evolution equations are postulated as

$$\boldsymbol{L}^{\mathrm{p}} := \dot{\boldsymbol{F}}^{\mathrm{p}} \cdot \boldsymbol{F}^{\mathrm{p}-1} = \lambda\, \partial_{\boldsymbol{\Sigma}}\Omega, \quad \dot{\boldsymbol{\alpha}} = \lambda\, \partial_{\boldsymbol{Q}}\Omega. \tag{35}$$

Though such equations do evidently not obey the classical principle of maximum dissipation, the second law of thermodynamics is a priori fulfilled, if Ω is convex (in $\boldsymbol{\Sigma}$ and $\boldsymbol{Q}$), cf. [29]. For non-linear hardening of Armstrong-Frederick-type

$$\Omega = \phi + \frac{1}{2}\,\frac{b}{c}\,\boldsymbol{Q} : \boldsymbol{Q}, \quad \Omega \neq \phi \tag{36}$$

is a suitable choice, see [29]. Application of Eq. (36) yields the evolution equations

$$\boldsymbol{L}^{\mathrm{p}} = \lambda\, \partial_{\boldsymbol{\Sigma}}\phi, \quad \dot{\boldsymbol{\alpha}} = -\lambda\, \partial_{\boldsymbol{\Sigma}}\phi - \lambda\, b\, \boldsymbol{\alpha}, \tag{37}$$

and finally, the dissipation inequality

$$\mathcal{D} = \lambda\, Q_0^{\mathrm{eq}} + \lambda\, \frac{b}{c}\, \boldsymbol{Q} : \boldsymbol{Q} \geq 0. \tag{38}$$

Accordingly, since Ω is convex, the predicted dissipation is non-negative. For a better understanding of the material parameters b and c the saturation behavior of Eqs. (37) is analyzed. By considering the limiting case $\dot{\boldsymbol{\alpha}} = \boldsymbol{0}$ the relations

$$||\boldsymbol{\alpha}|| \to \frac{||\partial_{\boldsymbol{\Sigma}}\phi||}{b}, \quad ||\boldsymbol{Q}|| \to c\, \frac{||\partial_{\boldsymbol{\Sigma}}\phi||}{b} \tag{39}$$

are obtained. Consequently, in case of a von Mises yield function of the type (34) implying $||\partial_{\boldsymbol{\Sigma}}\phi|| = 1$, Eqs. (39) yield $||\boldsymbol{\alpha}|| \to \frac{1}{b}$ and $||\boldsymbol{Q}|| \to \frac{c}{b}$. Furthermore, a purely isochoric evolution law is guaranteed then, i.e.,

$$\mathrm{tr}\boldsymbol{L}^{\mathrm{p}} = 0, \quad \mathrm{tr}\dot{\boldsymbol{\alpha}} = 0. \tag{40}$$

3.1.2 Implementational aspects

Most frequently, constitutive models such as those described in the previous paragraph are implemented by employing the classical return-mapping scheme, cf. [37, 38]. Hence, in case of a plastic loading step, the evolution equations (37) are integrated by utilizing an implicit backward-Euler integration and subsequently, the resulting non-linear algebraic system of equations is solved by applying Newton's methods. Here, the slightly different implicit first-order approximation

$$\boldsymbol{F}^{\mathrm{p}}_{n+1} = \exp(\Delta\lambda\, \partial_{\boldsymbol{\Sigma}}\phi) \cdot \boldsymbol{F}^{\mathrm{p}}_{n} \tag{41}$$

is considered for the flow rule. In contrast to a classical backward-Euler scheme, Eq. (41) preserves isochoric constraints exactly, cf. [37]. Contrariwise, the standard backward-Euler method resulting in

$$\boldsymbol{\alpha}_{n+1} = \frac{\boldsymbol{\alpha}_n - \Delta\lambda\, \partial_{\boldsymbol{\Sigma}}\phi}{1 + \Delta\lambda\, b} \tag{42}$$

is adopted for the back strain. It bears emphasis that other evolution equations based on objective time derivatives can be discretized similarly (compare to Eq. (32)). However, that will not be discussed in the present context. The nonlinear equations (41) and (42), together with the yield condition $\phi = 0$, are solved in a standard fashion. For instance, if $\Delta\lambda$ and $\boldsymbol{\Sigma}$ are chosen as unknowns, they result from the non-linear problem

$$\boldsymbol{R} = \boldsymbol{R}(\Delta\lambda, \boldsymbol{\Sigma}) = [\phi;\ \boldsymbol{R}^{\boldsymbol{F}^{\mathrm{p}}}] = \boldsymbol{0}, \qquad \boldsymbol{R}^{\boldsymbol{F}^{\mathrm{p}}} := -\boldsymbol{F}^{\mathrm{p}}_{n+1} + \exp(\Delta\lambda\, \partial_{\boldsymbol{\Sigma}}\phi) \cdot \boldsymbol{F}^{\mathrm{p}}_{n}. \tag{43}$$

3.2 Model II

The second geometrically non-linear extension of the original Armstrong-Frederick model presented here makes use of the so-called *center configuration*, originally proposed in [32] (see also [33] for further elaborations). Similar ideas have been advocated earlier in [34]. A comparison between this model and the one discussed before can be found in the present paper or in [31]. Following the structure of the previous section, the fundamentals are addressed first and subsequently, a brief comment on a standard numerical implementation by means of the return-mapping algorithm is given.

3.2.1 Fundamentals

In sharp contrast to Section 3.1 the non-linear kinematic hardening model advocated in [32] is based on the so-called center configuration induced by the additional multiplicative decomposition

$$\boldsymbol{F}^{\mathrm{p}} = \boldsymbol{F}^{\mathrm{k}^{-1}} \cdot \tilde{\boldsymbol{F}}^{\mathrm{k}}. \tag{44}$$

Physically speaking, $\boldsymbol{F}^{\mathrm{p}}$ does still represent the plastic deformation, while analogously, $\boldsymbol{F}^{\mathrm{k}}$ governs the possibly independent kinematic hardening effects (mapping between the center configuration and the standard intermediate configuration). By combining this interpretation with the objectivity condition, a Helmholtz energy of the type

$$\Psi = \Psi^{\mathrm{e}}(\boldsymbol{C}^{\mathrm{e}}) + \Psi^{\mathrm{p}}(\boldsymbol{C}^{\mathrm{k}}), \quad \boldsymbol{C}^{\mathrm{k}} := \boldsymbol{F}^{\mathrm{k}^{T}} \cdot \boldsymbol{F}^{\mathrm{k}} \tag{45}$$

is adopted. Accordingly and in line with the fundamentals of hyperelasticity, plastic hardening effects are defined by a potential. Consequently, this model naturally avoids oscillation problems as evident in some other approaches, cf. [32, 46]. Inserting Eqs. (44) and (45) into the dissipation inequality yields

$$\mathcal{D} = \boldsymbol{\Sigma} : \boldsymbol{L}^{\mathrm{p}} - \boldsymbol{Q}^{\mathrm{k}} : \boldsymbol{L}^{\mathrm{k}} \geq 0. \tag{46}$$

Here, the internal back stress $\boldsymbol{Q}^{\mathrm{k}}$ defined as

$$\boldsymbol{Q}^{\mathrm{k}} := 2\, \boldsymbol{C}^{\mathrm{k}} \cdot \frac{\partial \Psi^{\mathrm{p}}}{\partial \boldsymbol{C}^{\mathrm{k}}}, \quad \boldsymbol{L}^{\mathrm{k}} := \boldsymbol{F}^{\mathrm{k}^{-1}} \cdot \dot{\boldsymbol{F}}^{\mathrm{k}} \tag{47}$$

has been introduced. As expected, it shows the same structure as the Mandel stresses. This is a direct consequence of the similarity of $\Psi^{\mathrm{e}} = \Psi(\boldsymbol{F}^{\mathrm{e}})$ and $\Psi^{\mathrm{p}} = \Psi^{\mathrm{p}}(\boldsymbol{F}^{\mathrm{k}})$. The model is completed by postulating a yield function of the type

$$\phi = \Sigma^{\mathrm{eq}}(\boldsymbol{\Sigma} - \boldsymbol{Q}^{\mathrm{k}}) - Q_0^{\mathrm{eq}}, \tag{48}$$

together with evolution equations

$$\boldsymbol{L}^{\mathrm{p}} = \lambda\, \partial_{\boldsymbol{\Sigma}} \Omega, \quad \boldsymbol{L}^{\mathrm{k}} = -\lambda\, \partial_{\boldsymbol{Q}^{\mathrm{k}}} \Omega^{\mathrm{k}} \tag{49}$$

based on a plastic potential

$$\Omega^{\mathrm{k}} := \phi + \frac{1}{2}\,\frac{b}{c}\,\boldsymbol{Q}^{\mathrm{k}} : \boldsymbol{Q}^{\mathrm{k}}, \quad \Omega \neq \phi \tag{50}$$

being identical to that utilized in the previous subsection (compare to Eq. (36)). Consequently,

$$\boldsymbol{L}^{\mathrm{p}} = \lambda\, \partial_{\boldsymbol{\Sigma}} \phi, \quad \boldsymbol{L}^{\mathrm{k}} = \lambda \partial_{\boldsymbol{\Sigma}} \phi - \lambda\, \frac{b}{c}\, \boldsymbol{Q}^{\mathrm{k}}. \tag{51}$$

The dissipation predicted by that model is computed by inserting Eqs. (51) into the reduced dissipation, finally resulting in

$$\mathcal{D} = \lambda\, Q_0^{\mathrm{eq}} + \lambda\, \frac{b}{c}\, \boldsymbol{Q}^{\mathrm{k}} : \boldsymbol{Q}^{\mathrm{k}} \geq 0. \tag{52}$$

As in Section 3.1, convexity of Ω guarantees positive dissipation. More precisely, all equations such as Eq. (51) and Eq. (52) are formally identical to their counterparts presented in the previous subsection. Hence, in case of a von Mises-type model, the back stress inherits the isochoric property, i.e.,

$$\mathrm{tr}\boldsymbol{Q}^{\mathrm{k}} = 0. \tag{53}$$

Remark 3.1 *It bears emphasis that although both non-linear kinematic hardening approaches look similar, the material parameters b and c defining those models have a different physical interpretation. More precisely, by comparing the uniaxial tension test as predicted by those models it can be shown that the hardening parameters have to be divided by a factor of 2 for the approach related to the center configuration. Further details are omitted. They can be found in [44].*

3.2.2 Implementational aspects

In line with Paragraph 3.1.2, the implementation of the aforementioned plasticity model by means of the return-mapping algorithm is briefly discussed. Hence, an exponential implicit integration scheme is employed again for the irreversible parts of the deformation gradient, i.e.,

$$\boldsymbol{R}^{\boldsymbol{F}^{\mathrm{p}}} := -\boldsymbol{F}^{\mathrm{p}}_{n+1} + \exp(\Delta\lambda\, \partial_{\boldsymbol{\Sigma}} \phi) \cdot \boldsymbol{F}^{\mathrm{p}}_{n} = \boldsymbol{0} \tag{54}$$

and

$$\boldsymbol{R}^{\boldsymbol{F}^{\mathrm{k}}} := -\boldsymbol{F}^{\mathrm{k}}_{n+1} + \boldsymbol{F}^{\mathrm{k}}_{n} \cdot \exp\left[\Delta\lambda\, \partial_{\boldsymbol{\Sigma}} \phi - \Delta\lambda \frac{b}{c}\, \boldsymbol{Q}^{\mathrm{k}}\right] = \boldsymbol{0} \tag{55}$$

and finally, the unknowns such as $\Delta\lambda$, $\boldsymbol{\Sigma}$ and $\boldsymbol{Q}^{\mathrm{k}}$ are computed from the system of non-linear algebraic equations

$$\boldsymbol{R} = [\phi;\ \boldsymbol{R}^{\boldsymbol{F}^{\mathrm{p}}};\ \boldsymbol{R}^{\boldsymbol{F}^{\mathrm{k}}}] = \boldsymbol{0}, \qquad \boldsymbol{R} = \boldsymbol{R}(\Delta\lambda, \boldsymbol{\Sigma}, \boldsymbol{Q}^{\mathrm{k}}) = \boldsymbol{0}. \tag{56}$$

Alternatively, Eq. (55) could be enforced a priori (by a certain post-processing step, i.e., a staggered scheme) and hence, the reduced residual would read

$$\boldsymbol{R}_{\mathrm{red}} = \boldsymbol{R}_{\mathrm{red}}(\Delta\lambda, \boldsymbol{\Sigma}) = [\phi;\ \boldsymbol{R}^{\boldsymbol{F}^{\mathrm{p}}}] = \boldsymbol{0}. \tag{57}$$

Clearly, in this case, the post-processing step is defined by the non-linear subproblem

$$\boldsymbol{F}^{\mathrm{k}}_{n+1} = \boldsymbol{F}^{\mathrm{k}}_{n+1}(\Delta\lambda, \tilde{\boldsymbol{\Sigma}}). \tag{58}$$

Though such a procedure is not standard, it proves to be well suited for the variational constitutive update presented in the next section.

4 Variational updates for plasticity models with non-linear kinematic hardening

According to Section 2, the underlying idea of variational updates is the minimization of the integrated stress power. This variational principle governs every aspect of the respective physical problem. Unfortunately, the derivation of this scheme is based on the classical postulate of maximum dissipation which is not fulfilled for non-associative evolution equations. As a result, the original variational update cannot be applied to the class of non-linear hardening models as presented in the previous section. For this reason and in line with [28], an extended principle is considered. Conceptually, the integrated stress power is still minimized. However, by utilizing a suitable parameterization, the non-associative evolution equations are a priori prescribed. Interestingly, this parameterization results finally in an unconstrained minimization problem.

Following Section 2, the integrated stress power

$$\inf I_{\text{inc}}, \quad I_{\text{inc}} = \Psi_{n+1} - \Psi_n + \int_{t_n}^{t_{n+1}} \mathcal{D} \, \mathrm{d}t \tag{59}$$

represents the starting point of the extended variational constitutive updates. Since the dissipation as defined by Eq. (38) and that by Eq. (52) are formally identical, both models result eventually in a similar minimization problem. The numerical implementations discussed in the following subsections are based on a backward-Euler time discretization of the dissipation, i.e.,

$$\int_{t_n}^{t_{n+1}} \mathcal{D} \, \mathrm{d}t \approx \Delta\lambda Q_0^{\text{eq}} + \Delta\lambda \, \frac{b}{c} \, \boldsymbol{Q}_{n+1} : \boldsymbol{Q}_{n+1} =: \Delta\mathcal{D}. \tag{60}$$

Clearly, other (consistent) approximations are possible as well.

In Subsection 4.1, a variational constitutive update is developed for the non-linear kinematic hardening model as described in Subsection 3.1. A variational principle, together with its numerical implementation, for the model based on the center configuration as discussed in Subsection 3.2 is advocated in Subsection 4.2.

4.1 Model I

4.1.1 The continuous case: Differential equations

In line with Subsection 2, the stress power is considered. If linear kinematic hardening is replaced by the non-linear counterpart as described in Subsection 3.1, the stress power reads (compare to Eq. (18))

$$\begin{aligned} \mathcal{E}(\lambda, \tilde{\boldsymbol{\Sigma}}) &= -\left(\boldsymbol{F}^{\text{e}T} \cdot \frac{\partial \Psi^{\text{e}}}{\partial \boldsymbol{F}^{\text{e}}} \right) : \boldsymbol{L}^{\text{p}} + \boldsymbol{Q} : (\boldsymbol{L}^{\text{p}} + \lambda \, b \, \boldsymbol{\alpha}) + \lambda \, Q_0^{\text{eq}} + \lambda \, \frac{b}{c} \, \boldsymbol{Q} : \boldsymbol{Q} \\ &= (-\boldsymbol{\Sigma} + \boldsymbol{Q}) : \partial_{\boldsymbol{\Sigma}} \phi|_{\tilde{\boldsymbol{\Sigma}}} \, \lambda + Q_0^{\text{eq}} \, \lambda. \end{aligned} \tag{61}$$

Accordingly, a minimization of $\mathcal{E}$ with respect to the plastic multiplier yields

$$\begin{aligned} \delta_\lambda \mathcal{E} &= \{(-\boldsymbol{\Sigma} + \boldsymbol{Q}) : \partial_{\boldsymbol{\Sigma}} \phi|_{\tilde{\boldsymbol{\Sigma}}} + Q_0^{\text{eq}}\} \; \delta\lambda = 0 \\ &\Leftrightarrow \quad -\phi = 0. \end{aligned} \tag{62}$$

Consequently, the yield condition is consistently included within the variational (minimization) principle $\inf \mathcal{E}$. The stationarity condition with respect to the pseudo stresses is identical to that of the associative model (cf. Subsection 2). More precisely, a straightforward calculation leads to

$$\begin{array}{rcl} \delta_{\tilde{\boldsymbol{\Sigma}}} \mathcal{E} & = & \lambda \, \left\{ (-\boldsymbol{\Sigma} + \boldsymbol{Q}) : \partial^2_{\boldsymbol{\Sigma}} \phi|_{\tilde{\boldsymbol{\Sigma}}} \right\} : \delta \tilde{\boldsymbol{\Sigma}} = 0 \\ & \Leftrightarrow & \boldsymbol{\Xi} : \partial^2_{\boldsymbol{\Xi}} \phi = 0. \end{array} \tag{63}$$

As mentioned earlier, Eq. (63) is identically fulfilled, if the yield function is positively homogeneous of degree one, see [28]. Hence, the yield function and the flow direction predicted by the minimization principle $\inf \mathcal{E}$ are equivalent to those of the original (not variational) model (Subsection 3.1).

4.1.2 The discrete case: Time discretization

Next, consistency of the proposed variational constitutive update is proved. Hence, it will be shown that the minimization principle $\inf I_{\text{inc}}$ as defined by Eq. (59) converges to the underlying analytical counterpart $\inf \mathcal{E}$ for $\Delta t \to 0$. More precisely,

$$\left. \frac{\partial I_{\text{inc}}}{\partial \Delta\lambda} \right|_{\Delta t \to 0} \stackrel{!}{=} -\phi, \quad \left. \frac{\partial I_{\text{inc}}}{\partial \tilde{\boldsymbol{\Sigma}}} \right|_{\Delta t \to 0} \stackrel{!}{=} \boldsymbol{\Xi} : \partial^2_{\boldsymbol{\Xi}} \phi. \tag{64}$$

Since a variation is only considered for the (unknown) new state t_{n+1}, the index $n+1$ will be omitted in what follows, i.e., $\boldsymbol{\alpha} := \boldsymbol{\alpha}_{n+1}$.

For checking consistency, i.e., the validity of Eqs. (64), the partial derivatives

$$\frac{\partial \boldsymbol{\alpha}}{\partial \Delta\lambda} = \frac{-1}{1 + b \, \Delta\lambda} \, (\partial_{\boldsymbol{\Sigma}} \phi|_{\tilde{\boldsymbol{\Sigma}}} + b \, \boldsymbol{\alpha}) \tag{65}$$

$$\frac{\partial \boldsymbol{\alpha}}{\partial \tilde{\boldsymbol{\Sigma}}} = \frac{-\Delta\lambda}{1 + b \, \Delta\lambda} \, \partial^2_{\boldsymbol{\Sigma}} \phi\big|_{\tilde{\boldsymbol{\Sigma}}} \tag{66}$$

$$\frac{\partial \Psi^{\text{e}}}{\partial \Delta\lambda} = - \left[(\boldsymbol{F}^{\text{e}}_{\text{trial}})^T \cdot \frac{\partial \Psi^{\text{e}}}{\partial \boldsymbol{F}^{\text{e}}} \right] : D \exp \left[- \Delta\lambda \, \partial_{\boldsymbol{\Sigma}} \phi|_{\tilde{\boldsymbol{\Sigma}}} \right] : \partial_{\boldsymbol{\Sigma}} \phi|_{\tilde{\boldsymbol{\Sigma}}} \tag{67}$$

$$\frac{\partial \Psi^{\text{e}}}{\partial \tilde{\boldsymbol{\Sigma}}} = - \left[(\boldsymbol{F}^{\text{e}}_{\text{trial}})^T \cdot \frac{\partial \Psi^{\text{e}}}{\partial \boldsymbol{F}^{\text{e}}} \right] : D \exp \left[- \Delta\lambda \, \partial_{\boldsymbol{\Sigma}} \phi|_{\tilde{\boldsymbol{\Sigma}}} \right] : \partial^2_{\boldsymbol{\Sigma}} \phi\big|_{\tilde{\boldsymbol{\Sigma}}} \, \Delta\lambda \tag{68}$$

$$\frac{\partial \Psi^{\text{p}}}{\partial \Delta\lambda} = \frac{1}{1 + b \, \Delta\lambda} \, (\partial_{\boldsymbol{\Sigma}} \phi|_{\tilde{\boldsymbol{\Sigma}}} + b \, \boldsymbol{\alpha}) : \boldsymbol{Q} \tag{69}$$

$$\frac{\partial \Psi^{\text{p}}}{\partial \tilde{\boldsymbol{\Sigma}}} = \frac{\Delta\lambda}{1 + b \, \Delta\lambda} \, \boldsymbol{Q} : \partial^2_{\boldsymbol{\Sigma}} \phi\big|_{\tilde{\boldsymbol{\Sigma}}} \tag{70}$$

$$\frac{\partial \Delta\mathcal{D}}{\partial \Delta\lambda} = Q_0^{\text{eq}} - b \, \boldsymbol{Q} : \boldsymbol{\alpha} + 2 \, b \, \frac{\Delta\lambda}{1 + b \, \Delta\lambda} \, (\partial_{\boldsymbol{\Sigma}} \phi|_{\tilde{\boldsymbol{\Sigma}}} + b \, \boldsymbol{\alpha}) : \boldsymbol{Q} \tag{71}$$

$$\frac{\partial \mathcal{D}}{\partial \tilde{\boldsymbol{\Sigma}}} = 2 \, b \, \frac{\Delta\lambda^2}{1 + b \, \Delta\lambda} \, \boldsymbol{Q} : \partial^2_{\boldsymbol{\Sigma}} \phi\big|_{\tilde{\boldsymbol{\Sigma}}} \tag{72}$$

will be utilized. Here and henceforth, $\boldsymbol{F}^{\text{e}}_{\text{trial}} := \boldsymbol{F}_{n+1} \cdot \boldsymbol{F}_n^{\text{p}\,-1}$ are the elastic trial strains (see [37, 38]) and $D \exp(\bullet)$ is the derivative of the exponential mapping, cf. [47, 48]. By combining Eqs. (65)–(72), consistency of the algorithm can be verified, i.e.,

$$\left. \frac{\partial I_{\text{inc}}}{\partial \Delta\lambda} \right|_{\Delta t \to 0} = -\boldsymbol{\Sigma} : \partial_{\boldsymbol{\Sigma}} \phi|_{\tilde{\boldsymbol{\Sigma}}} + \boldsymbol{Q} : \partial_{\boldsymbol{\Sigma}} \phi|_{\tilde{\boldsymbol{\Sigma}}} + Q_0^{\text{eq}} = -\phi \tag{73}$$

and

$$\left.\frac{\partial I_{\text{inc}}}{\partial \tilde{\boldsymbol{\Sigma}}}\right|_{\Delta t\to 0} = \Delta\lambda\ \left[-\boldsymbol{\Sigma} : \partial^2_{\boldsymbol{\Sigma}}\phi\big|_{\tilde{\boldsymbol{\Sigma}}} + \boldsymbol{Q} : \partial^2_{\boldsymbol{\Sigma}}\phi\big|_{\tilde{\boldsymbol{\Sigma}}}\right] = \Delta\lambda\ \boldsymbol{\Xi} : \partial^2_{\boldsymbol{\Xi}}\phi. \tag{74}$$

In the numerical examples presented in Section 5, the minimization problem $\inf I_{\text{inc}}$ is solved by employing a gradient-type approach. Consequently, the function to be minimized, together with its gradient ∇I_{inc}, are required. Evidently, such gradient can easily be computed by Eqs. (65) – (72). In case of a Newton-type method, the second derivatives are required as well. Although they are very lengthy, they can be derived in a straightforward manner, cf. Remark 4.1. Having computed the minimization principle $\inf I_{\text{inc}}|_{\boldsymbol{F}} = \text{const}$, the stress can be computed analogously to hyperelasticity, i.e.,

$$\boldsymbol{P} = \partial_{\boldsymbol{F}} \inf_{\Delta\lambda,\tilde{\boldsymbol{\Sigma}}} I_{\text{inc}}, \tag{75}$$

compare to [24, 28].

4.2 Model II

4.2.1 The continuous case: Differential equations

Following the previous subsection, the analytical problem $\inf \mathcal{E}$ is analyzed first. Therefore, the stress power is computed. By employing Eq. (59) and Eq. (60), together with Subsection 3.2, the stress power results in

$$\begin{aligned}\mathcal{E}(\lambda,\tilde{\boldsymbol{\Sigma}}) &= \lambda\ \left\{-\boldsymbol{\Sigma} : \partial_{\boldsymbol{\Sigma}}\phi|_{\tilde{\boldsymbol{\Sigma}}} - \boldsymbol{Q}^{\text{k}} : \partial_{\boldsymbol{Q}^{\text{k}}}\Omega^{\text{k}} + Q_0^{\text{eq}} + \frac{b}{c}\,\boldsymbol{Q}^{\text{k}} : \boldsymbol{Q}^{\text{k}}\right\} \\ &= \lambda\ \left\{(-\boldsymbol{\Sigma} + \boldsymbol{Q}^{\text{k}}) : \partial_{\boldsymbol{\Sigma}}\phi|_{\tilde{\boldsymbol{\Sigma}}} + Q_0^{\text{eq}}\right\}.\end{aligned} \tag{76}$$

Thus, the related stationarity conditions are given by

$$\begin{aligned}\delta_\lambda\mathcal{E} &= \left\{(-\boldsymbol{\Sigma} + \boldsymbol{Q}^{\text{k}}) : \partial_{\boldsymbol{\Sigma}}\phi|_{\tilde{\boldsymbol{\Sigma}}} + Q_0^{\text{eq}}\right\}\ \delta\lambda = 0 \\ &\Leftrightarrow\ -\phi = 0\end{aligned} \tag{77}$$

and

$$\begin{aligned}\delta_{\tilde{\boldsymbol{\Sigma}}}\mathcal{E} &= \lambda\ \left\{(-\boldsymbol{\Sigma} + \boldsymbol{Q}^{\text{k}}) : \partial^2_{\boldsymbol{\Sigma}}\phi|_{\tilde{\boldsymbol{\Sigma}}}\right\} : \delta\tilde{\boldsymbol{\Sigma}} = 0 \\ &\Leftrightarrow\ \boldsymbol{\Xi} : \partial^2_{\boldsymbol{\Xi}}\phi = 0.\end{aligned} \tag{78}$$

As a result and analogously to the previous subsection, the proposed minimization principle is equivalent to its underlying (non-variational) counterpart as summarized in 3.2.

4.2.2 The discrete case: Time discretization

Consistency of the variational constitutive update as obtained from discretizing the integrated stress power (76) by utilizing a backward-Euler integration is checked here. According to Paragraph 3.2.2 and in contrast to Subsection 4.1, a standard parameterization of the minimization principle would require 3 unknowns: $\Delta\lambda$, $\tilde{\boldsymbol{\Sigma}}$ and additionally, the direction of $\boldsymbol{L}^{\text{k}}$. Clearly, this could be done by introducing an additional set of pseudo stresses defining $\boldsymbol{L}^{\text{k}}$. However, a different approach is elaborated here. In line with the modified return-mapping scheme presented in Paragraph 3.2.2, the evolution equation governing $\boldsymbol{F}^{\text{k}}$ is a priori fulfilled by enforcing

$$\boldsymbol{F}^{\text{k}}_{n+1} = \boldsymbol{F}^{\text{k}}_{n+1}(\Delta\lambda,\tilde{\boldsymbol{\Sigma}}). \tag{79}$$

By doing so, the only unknowns within the minimization principle $\inf I_{\mathrm{inc}}$ are $\Delta\lambda$ and $\tilde{\boldsymbol{\Sigma}}$ – the same as in the previous subsection. Hence, both algorithms are easily mutually comparable. In what follows, the flow direction and the hardening directions are denoted by

$$\boldsymbol{N} := \partial_{\boldsymbol{\Sigma}}\phi|_{\tilde{\boldsymbol{\Sigma}}}\,, \quad \hat{\boldsymbol{N}} := \partial_{\boldsymbol{\Sigma}}\phi|_{\tilde{\boldsymbol{\Sigma}}} - \frac{b}{c}\,\boldsymbol{Q}^{\mathrm{k}}. \tag{80}$$

Since both models for non-linear kinematic hardening considered in this paper lead to the same elastic part of the Helmholtz energy Ψ^{e} (and the same plastic flow rule), the derivatives $\partial_{\Delta\lambda}\Psi^{\mathrm{e}}$ and $\partial_{\tilde{\boldsymbol{\Sigma}}}\Psi^{\mathrm{e}}$ are given by Eq. (67) and Eq. (68). The remaining derivatives necessary for solving the minimization problem I_{inc} by using gradient-type algorithms are summarized in what follows.

With Eqs. (80), the derivative of $\boldsymbol{F}^{\mathrm{k}}$ with respect to the plastic multiplier can be computed from the implicit equation

$$\frac{\partial \boldsymbol{F}^{\mathrm{k}}_{n+1}}{\partial\Delta\lambda} = \boldsymbol{F}^{\mathrm{k}}_{n} \cdot \left[D\exp\left(\Delta\lambda\,\hat{\boldsymbol{N}}\right) : \left(\hat{\boldsymbol{N}} + \Delta\lambda\,\partial_{\Delta\lambda}\hat{\boldsymbol{N}}\right)\right]. \tag{81}$$

For that purpose, the derivative

$$\partial_{\Delta\lambda}\hat{\boldsymbol{N}} = -\frac{b}{c}\,\partial_{\boldsymbol{F}^{\mathrm{k}}}\boldsymbol{Q}^{\mathrm{k}} : \partial_{\Delta\lambda}\boldsymbol{F}^{\mathrm{k}} \tag{82}$$

is inserted into Eq. (81), leading finally to

$$\frac{\partial \boldsymbol{F}^{\mathrm{k}}_{n+1}}{\partial\Delta\lambda} = \mathbb{A}^{-1} : \left[\boldsymbol{F}^{\mathrm{k}}_{n} \cdot D\exp\left(\Delta\lambda\,\hat{\boldsymbol{N}}\right) : \hat{\boldsymbol{N}}\right]. \tag{83}$$

Here, the fourth-order tensor

$$\mathbb{A} = \mathbb{I} + \Delta\lambda\,\frac{b}{c}\,\boldsymbol{F}^{\mathrm{k}}_{n} \cdot D\exp\left(\Delta\lambda\,\hat{\boldsymbol{N}}\right) : \partial_{\boldsymbol{F}^{\mathrm{k}}}\boldsymbol{Q}^{\mathrm{k}} \tag{84}$$

has been introduced. Evidently, Eq. (82) can only be applied, if the evolution direction defining $\boldsymbol{L}^{\mathrm{k}}$ is correct. This is why Eq. (79) has to be enforced. Analogously, the derivative of $\boldsymbol{F}^{\mathrm{k}}$ with respect to the pseudo stresses can be computed. More precisely,

$$\frac{\partial \boldsymbol{F}^{\mathrm{k}}_{n+1}}{\partial\tilde{\boldsymbol{\Sigma}}} = \Delta\lambda\,\mathbb{A}^{-1} : \left[\boldsymbol{F}^{\mathrm{k}}_{n} \cdot D\exp\left(\Delta\lambda\,\hat{\boldsymbol{N}}\right) : \partial^2_{\boldsymbol{\Sigma}}\phi\big|_{\tilde{\boldsymbol{\Sigma}}}\right]. \tag{85}$$

Hence, the gradients of Ψ^{p} and those of $\Delta\mathcal{D}$ are given by

$$\frac{\partial\Psi^{\mathrm{p}}}{\partial\Delta\lambda} = \frac{\partial\Psi^{\mathrm{p}}}{\partial \boldsymbol{F}^{\mathrm{k}}_{n+1}} : \frac{\partial \boldsymbol{F}^{\mathrm{k}}_{n+1}}{\partial\Delta\lambda} \tag{86}$$

$$\frac{\partial\Psi^{\mathrm{p}}}{\partial\tilde{\boldsymbol{\Sigma}}} = \frac{\partial\Psi^{\mathrm{p}}}{\partial \boldsymbol{F}^{\mathrm{k}}_{n+1}} : \frac{\partial \boldsymbol{F}^{\mathrm{k}}_{n+1}}{\partial\tilde{\boldsymbol{\Sigma}}} \tag{87}$$

$$\frac{\partial\Delta\mathcal{D}}{\partial\Delta\lambda} = Q_0^{\mathrm{eq}} + \frac{b}{c}\,\boldsymbol{Q}^{\mathrm{k}} : \boldsymbol{Q}^{\mathrm{k}} + 2\,\Delta\lambda\,\frac{b}{c}\,\boldsymbol{Q}^{\mathrm{k}} : \frac{\partial \boldsymbol{Q}^{\mathrm{k}}}{\partial \boldsymbol{F}^{\mathrm{k}}_{n+1}} : \frac{\partial \boldsymbol{F}^{\mathrm{k}}_{n+1}}{\partial\Delta\lambda} \tag{88}$$

$$\frac{\partial\Delta\mathcal{D}}{\partial\tilde{\boldsymbol{\Sigma}}} = 2\,\Delta\lambda\,\frac{b}{c}\,\boldsymbol{Q}^{\mathrm{k}} : \frac{\partial \boldsymbol{Q}^{\mathrm{k}}}{\partial \boldsymbol{F}^{\mathrm{k}}_{n+1}} : \frac{\partial \boldsymbol{F}^{\mathrm{k}}_{n+1}}{\partial\tilde{\boldsymbol{\Sigma}}}. \tag{89}$$

By utilizing such gradients, together with Eq. (67) and Eq. (68), the gradient of I_{inc} required for an optimization scheme can be computed. In case of a Newton-type method, the second derivatives are necessary as well. Although they are lengthy, they can be derived in a straightforward manner, cf. Remark 4.1. Once this minimization problem has been solved, the stresses follow again from Eq. (75).

Next, consistency of the resulting algorithm is proved. By considering the linearizations

$$\left.\frac{\partial \boldsymbol{F}^{\text{k}}_{n+1}}{\partial \Delta\lambda}\right|_{\Delta t\to 0} = \boldsymbol{F}^{\text{k}}_{n+1}\cdot\hat{\boldsymbol{N}} \tag{90}$$

and

$$\left.\frac{\partial \boldsymbol{F}^{\text{k}}_{n+1}}{\partial \tilde{\boldsymbol{\Sigma}}}\right|_{\Delta t\to 0} = \Delta\lambda\ \boldsymbol{F}^{\text{k}}_{n+1}\cdot\partial^2_{\boldsymbol{\Sigma}}\phi\big|_{\tilde{\boldsymbol{\Sigma}}} \tag{91}$$

the stationarity conditions

$$\left.\frac{\partial I_{\text{inc}}}{\partial \Delta\lambda}\right|_{\Delta t\to 0} = \underbrace{-\boldsymbol{\Sigma}:\partial_{\boldsymbol{\Sigma}}}_{=\partial_{\Delta\lambda}\Psi^{\text{e}}|_{\Delta t\to 0}} + \underbrace{\boldsymbol{Q}^{\text{k}}:\hat{\boldsymbol{N}}}_{=\partial_{\Delta\lambda}\Psi^{\text{p}}|_{\Delta t\to 0}} + \underbrace{Q_0^{\text{eq}}+\frac{b}{c}\,\boldsymbol{Q}^{\text{k}}:\boldsymbol{Q}^{\text{k}}}_{=\partial_{\Delta\lambda}\Delta\mathcal{D}|_{\Delta t\to 0}} = -\phi = 0 \tag{92}$$

and

$$\left.\frac{\partial I_{\text{inc}}}{\partial \tilde{\boldsymbol{\Sigma}}}\right|_{\Delta t\to 0} = \underbrace{-\Delta\lambda\ \boldsymbol{\Sigma}:\partial_{\boldsymbol{\Sigma}}\phi|_{\tilde{\boldsymbol{\Sigma}}}}_{=\partial_{\tilde{\boldsymbol{\Sigma}}}\Psi^{\text{e}}|_{\Delta t\to 0}} + \underbrace{\Delta\lambda\ \boldsymbol{Q}^{\text{k}}:\partial_{\boldsymbol{\Sigma}}\phi|_{\tilde{\boldsymbol{\Sigma}}}}_{=\partial_{\tilde{\boldsymbol{\Sigma}}}\Psi^{\text{p}}|_{\Delta t\to 0}} = \Delta\lambda\ \boldsymbol{\Xi}:\partial_{\boldsymbol{\Sigma}}\phi|_{\boldsymbol{\Xi}} = \boldsymbol{0} \tag{93}$$

are finally obtained. In Eq. (93), $\partial_{\tilde{\boldsymbol{\Sigma}}}\Delta\mathcal{D}|_{\Delta t\to 0}=\boldsymbol{0}$ has already been included, see Eq. (89). Hence, consistency of the algorithm is guaranteed.

Remark 4.1 *As a prototype implementation, the optimization problems associated with model I and model II are solved by means of a gradient-type approach. More precisely, a so-called L-BFGS algorithm is applied, cf. [49]. The gradients necessary for this approach have been already derived in the present paper. Clearly, the performance of the resulting numerical implementation is strongly affected by the choice of the optimization algorithm. For a faster convergence, Newton's method could be employed as well. In this case, the Hessian of the function to be minimized would be required as well. Furthermore, the so-called algorithmic tangent moduli would be required for guaranteeing an asymptotic quadratic convergence also at the structural level. For this reason, the derivation of those tangent moduli will be sketched in what follows.*
Independently if model I or model II is considered, an optimization problem of the type

$$\inf_{\boldsymbol{X}} I_{\text{inc}}(\boldsymbol{F}_{n+1},\boldsymbol{X})|_{\boldsymbol{F}_{n+1}=\text{const}}, \quad \textit{with} \quad \boldsymbol{X}=\{\tilde{\boldsymbol{\Sigma}},\Delta\lambda\} \tag{94}$$

has to be solved. Having computed the minimum, the necessary condition

$$\partial_{\boldsymbol{X}} I_{\text{inc}}|_{\boldsymbol{F}_{n+1}=\text{const}} = \boldsymbol{0} \tag{95}$$

is obviously fulfilled. In line with the return-mapping scheme, the algorithmic tangent is derived by linearizing the residuals, i.e., the gradient of the function to be minimized. A straightforward computation gives

$$d(\partial_{\boldsymbol{X}} I_{\text{inc}}) = \boldsymbol{0} \quad \Rightarrow \quad d\boldsymbol{X} = -\left[\partial^2_{\boldsymbol{X}\boldsymbol{X}} I_{\text{inc}}\right]^{-1}\cdot\partial^2_{\boldsymbol{X}\boldsymbol{F}} I_{\text{inc}} : d\boldsymbol{F}. \tag{96}$$

Note that in contrast to the minimization problem (94), the deformation gradient is now a non-constant variable. Inserting this equation into the linearization of the stress tensor $\boldsymbol{P} = \partial_{\boldsymbol{F}} I_{\text{inc}}$*, leads finally to*

$$d\boldsymbol{P} = \underbrace{\left\{ \partial^2_{\boldsymbol{F}\boldsymbol{F}} I_{\text{inc}} - \partial^2_{\boldsymbol{F}\boldsymbol{X}} I_{\text{inc}} \cdot \left[\partial^2_{\boldsymbol{X}\boldsymbol{X}} I_{\text{inc}}\right]^{-1} \cdot \partial^2_{\boldsymbol{X}\boldsymbol{F}} I_{\text{inc}} \right\}}_{:= \mathbb{A}} : d\boldsymbol{F}. \tag{97}$$

Accordingly and as expected, the tangent operator $\mathbb{A}$ *shows the major symmetry for a variational method.*

5 Numerical examples

The applicability as well as the consistency of the proposed variational constitutive updates are demonstrated in this section by means of different numerical examples. While Subsection 5.1 is associated with the uniaxial tension and the simple shear test, a more complex boundary value problem is considered in Subsection 5.2. To be more precise, it is a strip with a circular hole.

The minimization principle (59) characterizing the novel variational constitutive updates is solved by means of a gradient-based L-BFGS algorithm, cf. [49]. In line with the standard return-mapping scheme, the initial values necessary for this algorithm are chosen as those corresponding to an elastic predictor. The respective constitutive subroutine has been embedded into an in-house finite element code. Within this code, the global problem (equilibrium) is solved by energy minimization as well, i.e., the L-BFGS algorithm is also applied at that scale. However, the implementation of the constitutive models can easily be inserted into commercial finite element package as well. Within all optimization algorithms, convergence is checked by the projected gradient and the tolerance is set to 10^{-8}, cf. [49].

5.1 Uniaxial tension and simple shear

The representative hardening behavior corresponding to the Armstrong-Frederick-type model can be visualized best by analyzing one loading cycle for simple shear or uniaxial tension. Following [31], the material parameters characterizing a mild steel CK15 are chosen. They are summarized below.

shear modulus:	$\mu = 80000$ MPa
bulk modulus:	$K = 173333$ MPa
yield stress:	$Q_0^{\text{eq}} = \sqrt{2/3}\, 300$ MPa
hardening modulus:	$c = 1900$ MPa
saturation parameter:	$b = 8.5$

As already mentioned in Remark 3.1, the hardening parameters have to be divided by a factor of 2 for the model based on the center configuration. Concerning the elastic response, a standard isotropic neo-Hooke-type Helmholtz energy is adopted. However, since the elastic strains are relatively small, the choice of the elasticity model is not crucial.

The predicted stress-strain responses for the two different loading cases are shown in Fig. 1. As evident from these diagrams, both proposed variational constitutive updates lead to almost identical results. This holds particularly for the simple shear test.

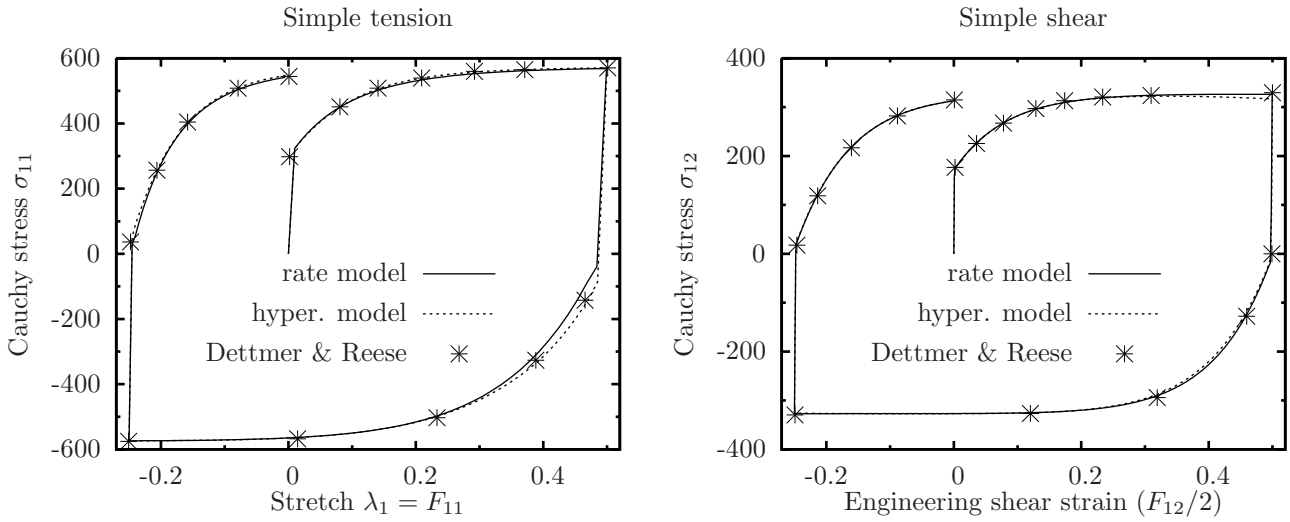

Figure 1: Uniaxial tension and simple shear test: Comparison between different finite strain plasticity models. *Rate model* is based on the standard evolution equation of the internal variables (see Subsection 3.1), while *hyper. model* is based on the kinematics associated with the center configuration (see Subsection 3.2). For the sake of comparison, the results as reported in [31] are shown as well.

no hardening:	perfect plasticity, i.e., $c = 0.0$
linear hardening:	Prager-Ziegler model, i.e., $\dot{\boldsymbol{\alpha}} = \boldsymbol{L}^{\mathrm{p}}$
rate model:	Armstrong-Frederick-type hardening based on standard rate equation (see Subsection 3.1), $c = c_{\mathrm{ref}}$, $b = b_{\mathrm{ref}}$
hyper. model:	Armstrong-Frederick-type hardening based on center configuration (see Subsection 3.2), $c = c_{\mathrm{ref}}/2$, $b = b_{\mathrm{ref}}/2$

Table 1: Strip with a circular hole: Different hardening models utilized within the numerical analyses

According to Fig. 1, the results are in good agreement to those previously reported in [31].

5.2 A strip with a circular hole

Next, a more complex mechanical problem characterized by an inhomogeneous stress state is numerically analyzed. The strip with a circular hole shown in Fig. 2 represents a standard benchmark being frequently applied to investigate the consistency of plasticity models, cf. [38, 50]. For the purpose of comparison, the material model is chosen in line with that in [38, 50], i.e., isotropic elasticity and associative von Mises plasticity theory. As in the previous examples, the elastic strains are relatively small. Thus, the choice of the elasticity model does not play an important role. For this reason and in line with the previous subsection, an isotropic neo-Hooke-type model is adopted. In contrast to the cited references, where only linear hardening was considered, the four different hardening models summarized in Tab. 1 are applied.

The distributions of the internal variable $\alpha := \max_{ij} |\alpha_{ij}|$ as predicted by the different hardening models are given in Fig. 3. As evident from this figure all computations lead

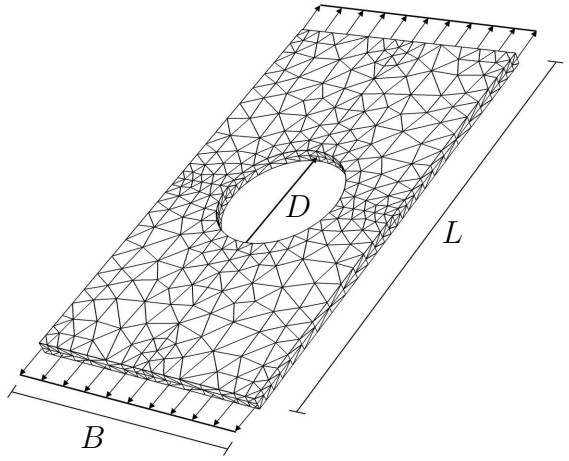

Geometry [cm]:		
L	36	
B	20	
D	10	
t	1.0	
Material parameters:		
E	70	kN/cm^2
ν	0.2	cm
Q_0^{eq}	$\sqrt{2/3}$ 0.242	kN/cm^2
c_{ref}	$\sqrt{2/3}$ 0.2	kN/cm^2
b_{ref}	1.0	-

Figure 2: Strip with a circular hole: geometry, boundary conditions, finite element discretization (10-node purely displacement-driven tetrahedron elements) and material parameters. t denotes the thickness.

to almost identical results. This is in line with [24]. In the cited paper, only a marginal influence of the hardening behavior on the distribution of α was observed (linear isotropic hardening and linear kinematic hardening were analyzed).

Although all different hardening models lead to similar distributions of the internal variable α, the resulting load-displacement diagrams show a larger scattering, cf. Fig. 3. As expected, the model without hardening predicts the softest response. Due to geometrical nonlinearities, the forces are monotonically decreasing beyond the ultimate load. The other limiting case, i.e., the strongest hardening effect, is represented by linear kinematic hardening. Again a global softening behavior is observed at large deformations. However, in contrast to perfect plasticity, the softening is less pronounced (different modulus) and occurs at a later stage. The proposed novel constitutive updates based on nonlinear kinematic hardening of Armstrong-Frederick-type are bounded by the aforementioned limiting cases. More precisely, they lead to identical results as the linear hardening model at the onset of plasticity, while for large deformations, i.e., when the internal variable $\boldsymbol{\alpha}$ has already saturated, the global softening modulus is identical to that of perfect plasticity. Clearly, this transition is consistent with the underlying theory. Although both models based on nonlinear kinematic hardening give reasonable results, their force-displacement curves are not completely identical. In contrast to the simple shear test and uniaxial tension, the difference between the models is more pronounced. The reason for this is the comparably higher strain level ($\alpha := \max_{ij} |\alpha_{ij}|| \approx 2$, see Fig. 3). Furthermore, differences between similar Armstrong-Frederick-type formulations have already been reported earlier, cf. [31].

For the sake of comparison, the load-displacement diagrams computed by applying a standard return-mapping scheme are shown in Fig. 4 as well. Accordingly, both schemes (the return-mapping procedure and the novel variational constitutive update) predict the same mechanical response. However, it is important to note that these algorithms are not equivalent.

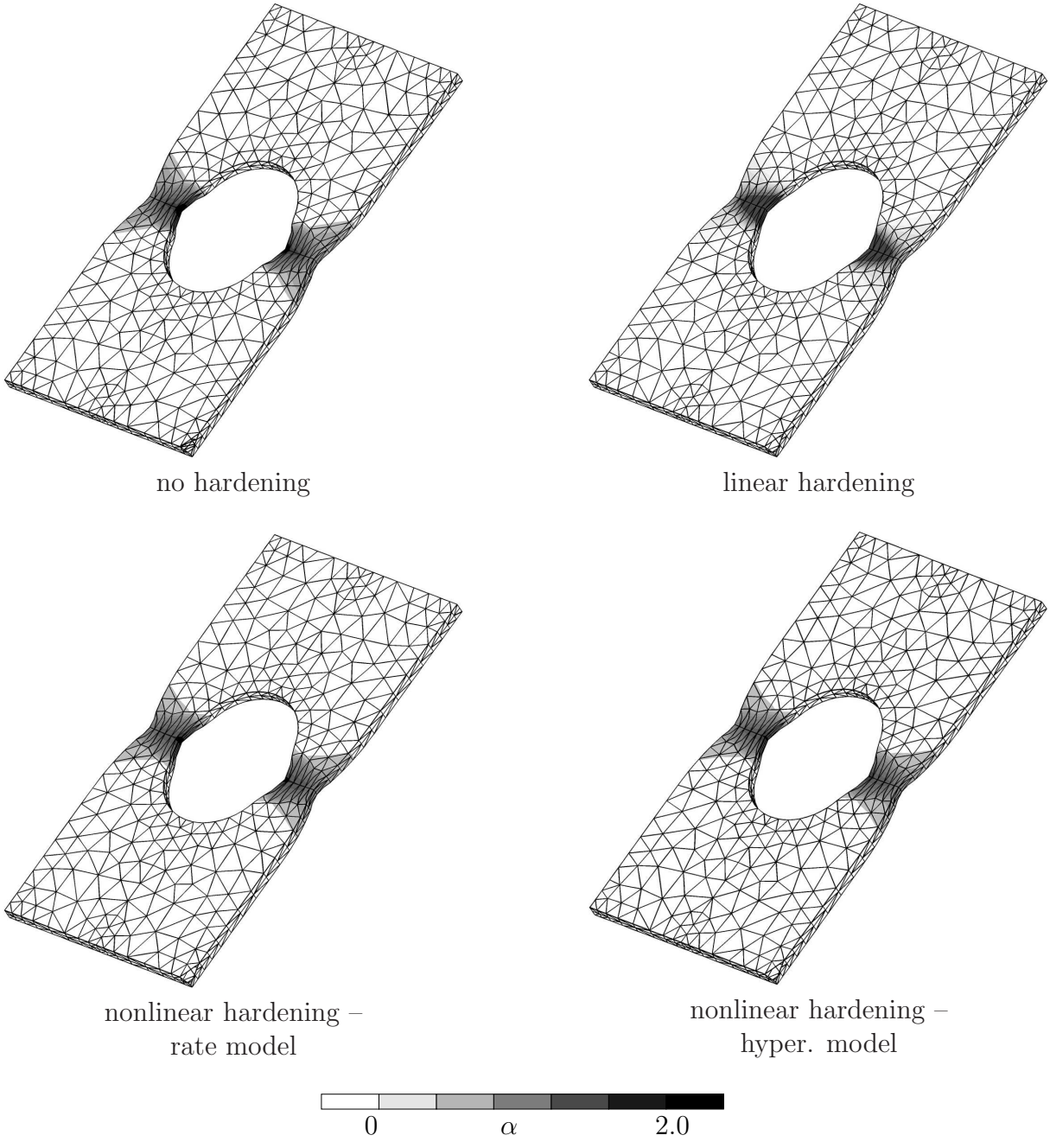

Figure 3: Strip with a hole: Distribution of the internal variable $\alpha := \max |\alpha_{ij}|$. Comparison between different finite strain plasticity models. *Rate model* is based on the standard evolution equation of the internal variables (see Subsection 3.1), while *hyper. model* is based on the kinematics associated with the center configuration (see Subsection 3.2).

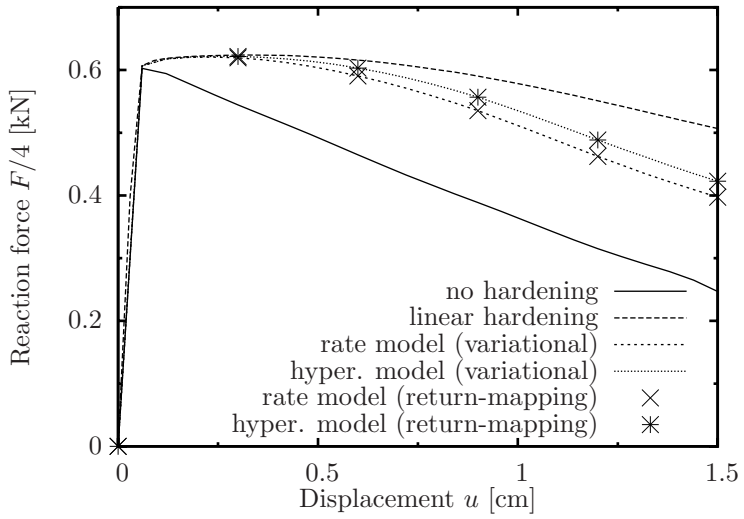

Figure 4: Strip with a hole: Load-displacement diagrams predicted by different finite strain plasticity models. *Rate model* is based on the standard evolution equation of the internal variables (see Subsection 3.1), while *hyper. model* is based on the kinematics associated with the center configuration (see Subsection 3.2).

6 Conclusions

In this paper, non-linear kinematic hardening of Armstrong-Frederick-type at finite strains was critically analyzed and recast into a variationally consistent framework. Within this framework, all unknown state variables, together with the deformation mapping, follow jointly from minimizing a suitable energy potential. In line with standard dissipative solids, i.e., solids governed by associative evolution equations, this energy potential is given by the (integrated) stress power. By utilizing a well adapted parameterization, the non-associative evolution equations defining the class of non-linear kinematic hardening models of Armstrong-Frederick-type were naturally enforced and incorporated in the minimization principle. By doing so, an equivalent unconstrained minimization problem was developed. Since, the extension of the original Armstrong-Frederick model to finite strains is not unique, two different approaches were considered and consistency of the resulting variational constitutive updates was proved. Numerical benchmarks showed the consistency of the advocated numerical implementations.
This is the second variational constitutive update proposed for a class of non-associative plasticity theory. However, it is not clear yet, which conditions have to be fulfilled in general such that an extended variational principle exists. Hence, in the future existence conditions are to be carefully derived.

References

[1] O.D. Jones. *Analytical Mechanics for Relativity and Quantum Mechanics*. Oxford Univ. Press, 2005.

[2] C. Papenfuss and W. Muschik. Evolution criterion in nonequilibrium and a variational principle for equilibrium states of free-standing liquid crystals. *Phys. Rev. E*, 56:4275, 1997.

[3] L. Onsager. Reciprocal relations in irreversible processes. *I. Phys. Rev.*, 37:405–426, 1931.

[4] L. Onsager. Theories and problems of liquid diffusion. *Ann. NY Acad. Sci.*, 46:241–265, 1945.

[5] J.E. Marsden and T.J.R. Hughes. *Mathematical foundation of elasticity*. Dover, New York, 1994.

[6] G. Dal Maso. *An introduction to* Γ*-convergence*. Birkhäuser, Boston, 1983.

[7] A. Braides. *Gamma-convergence for Beginners*. Oxford University Press, 2002.

[8] G. Dal Maso and C. Zanini. Quasistatic crack growth for a cohesive zone model with prescribed crack path. *Proc. Roy. Soc. Edinburgh Sect. A*, 137A:253–279, 2007.

[9] P. Thoutireddy and M. Ortiz. A variational r-adaption and shape-optimization method for finite-deformation elasticity. *International Journal for Numerical Methods in Engineering*, 61:1–21, 2004.

[10] J. Mosler. *On the numerical modeling of localized material failure at finite strains by means of variational mesh adaption and cohesive elements*. Habilitation, Ruhr University Bochum, Germany, 2007.

[11] R. Radovitzky and M. Ortiz. Error estimation and adaptive meshing in strongly nonlinear dynamic problems. *Computer Methods in Applied Mechanics and Engineering*, 172:203–240, 1999.

[12] J. Mosler and M. Ortiz. On the numerical implementation of variational arbitrary Lagrangian-Eulerian (VALE) formulations. *International Journal for Numerical Methods in Engineering*, 67:1272–1289, 2006.

[13] M. Ortiz and L. Stainier. The variational formulation of viscoplastic constitutive updates. *Computer Methods in Applied Mechanics and Engineering*, 171:419–444, 1999.

[14] E. Hairer and C. Lubich. Long-time energy conservation of numerical methods for oscillatory differential equations. *SIAM Journal of Numerical Analysis*, 38(2):414–441, 2000.

[15] J.E. Marsden and M. West. Discrete mechanics and variational integrators. *Acta Numerica*, 2001. in press.

[16] B. Halphen and Q.S. Nguyen. Sur les matériaux standards généralisés. *J. Méchanique*, 14:39–63, 1975.

[17] C. Comi, A. Corigliano, and G. Maier. Extremum properties of finite-step solutions in elastoplasticity with nonlinear hardening. *International Journal for Solids and Structures*, 29:965–981, 1991.

[18] C. Comi, G. Maier, and U. Perego. Generalized variable finite element modeling and extremum theorems in stepwise holonomic elastoplasticity with internal variables. *Computer Methods in Applied Mechanics and Engineering*, 96:213–237, 1992.

[19] C. Comi and U. Perego. A unified approach for variationally consistent finite elements in elastoplasticity. *Computer Methods in Applied Mechanics and Engineering*, 121:323–344, 1995.

[20] C. Carstensen, K. Hackl, and A. Mielke. Non-convex potentials and microstructures in finite-strain plasticity. *Proc. R. Soc. Lond. A*, 458:299–317, 2002.

[21] C. Miehe. Strain-driven homogenization of inelastic microstructures and composites based on an incremental variational formulation. *International Journal for Numerical Methods in Engineering*, 55:1285–1322, 2002.

[22] J.M. Ball. Convexity conditions and existence theorems in nonlinear elasticity. *Arch. Rat. Mech. Anal.*, 63:337–403, 1978.

[23] M. Ortiz and E.A. Repetto. Nonconvex energy minimisation and dislocation in ductile single crystals. *J. Mech. Phys. Solids*, 47:397–462, 1999.

[24] J. Mosler and O.T. Bruhns. On the implementation of rate-independent standard dissipative solids at finite strain – Variational constitutive updates. *Computer Methods in Applied Mechanics and Engineering*, 199:417–429, 2010.

[25] E. Fancello, J.-P. Ponthot, and L. Stainier. A variational formulation of constitutive models and updates in non-linear finite viscoelasticity. *International Journal for Numerical Methods in Engineering*, 65:1831–1864, 2006.

[26] J. Mandel. *Plasticité Classique et Viscoplasticité*. Cours and Lectures au CISM No. 97. International Center for Mechanical Sciences, Springer-Verlag, New York, 1972.

[27] J. Lemaitre. A continuous damage mechanics model for ductile fracture. *J. Eng. Mat. Techn.*, 107:83–89, 1985.

[28] J. Mosler and O.T. Bruhns. Towards variational constitutive updates for non-associative plasticity models at finite strain: models based on a volumetric-deviatoric split. *International Journal for Solids and Structures*, 46:1676–1684, 2009.

[29] J. Lemaitre and J.-L. Chaboche. *Mechanics of Solid Materials*. Cambridge University Press, 1994.

[30] F. Armstrong and C.O. Frederick. A mathematical representation of the multiaxial Bauschinger effect. C.E.G.B. Report RD/B/N731, Berkeley Nuclear Laboratories, 1966.

[31] W. Dettmer and S. Reese. On the theoretical and numerical modeling of armstrong-frederick kinematic hardening in the finite strain regime. *Computer Methods in Applied Mechanics and Engineering*, 193:87–116, 2004.

[32] M. Wallin, M. Ristinmaa, and N.S. Ottosen. Kinematic hardening in large strain plasticity. *Eur. J. Mech. A/Solids*, 22:341–356, 2003.

[33] A. Menzel, M. Ekh, K. Runesson, and P. Steinmann. A framework for multiplicative elastoplasticity with kinematic hardening coupled to anisotropic damage. *International Journal of Plasticity*, 21:371–434, 2005.

[34] A. Lion. Constitutive modelling in finite thermoviscoplasticity: a physical approach based on nonlinear rheological models. *International Journal of Plasticity*, 16:469–494, 2000.

[35] E.H. Lee. Elastic-plastic deformation at finite strains. *Journal of Applied Mechanics*, 36:1–6, 1969.

[36] J. Lubliner. *Plasticity theory*. Maxwell Macmillan International Edition, 1997.

[37] J.C. Simo. Numerical analysis of classical plasticity. In P.G. Ciarlet and J.J. Lions, editors, *Handbook for numerical analysis*, volume IV. Elsevier, Amsterdam, 1998.

[38] J.C. Simo and T.J.R. Hughes. *Computational inelasticity*. Springer, New York, 1998.

[39] B.D. Coleman and W. Noll. The thermodynamics of elastic materials with heat conduction and viscosity. *Arch. Rational Mech. Anal.*, 13:167178, 1963.

[40] B.D. Coleman. Thermodynamics of materials with memory. *Arch. Rational Mech. Anal.*, 17:1–45, 1964.

[41] B.D. Coleman and M.E. Gurtin. Thermodynamics with internal state variables. *J. Chem. Phys*, 47:597–613, 1967.

[42] A.M. Maugin. *The thermodynamics of Plasticity and Fracture*. Cambridge University Press, 1992.

[43] Ch. Tsakmakis. *Über inkrementelle Materialgleichungen zur Beschreibung großer inelastischer Verformungen*. PhD thesis, TU Darmstadt, 1987.

[44] O. Kintzel. *Modellierung elasto-plastischen Materialverhaltens und duktiler Porenschädigung metallischer Werkstoffe bei großen Deformationen*. PhD thesis, Ruhr University Bochum, 2007.

[45] O.T. Bruhns, H. Xiao, and A. Meyers. Some basic issues in traditional Eulerian formulations of finite elastoplasticity. *International Journal of Plasticity*, 19:2007–2026, 2003.

[46] J.K. Dienes. On the analysis of rotation and stress rate in deforming bodies. *Acta Mech.*, 32:217232, 1979.

[47] M. Ortiz, R.A. Radovitzky, and E.A. Repetto. The computation of the exponential and logarithmic mappings and their first and second linearizations. *International Journal for Numerical Methods in Engineering*, 52(12):1431–1441, 2001.

[48] M. Itskov. Computation of the exponential and other isotropic tensor functions and their derivatives. *Computer Methods in Applied Mechanics and Engineering*, 192(35-36):3985–3999, 2003.

[49] D.C. Liu and J. Nocedal. On the limited memory method for large scale optimization. *Mathematical Programming B*, 45(3):503–528, 1989.

[50] P. Fuschi, D. Perić, and D.R.J. Owen. Studies on generalized midpoint integration in rate-independent plasticity with reference to plane stress J_2-flow theory. *Computers & Structures*, 43:1117–1133, 1992.